Interaction of Optical and EHF Waves With VO_2 Nanosized Films and Particles

Alexander P. Kamantsev, Victor V. Koledov, Vladimir G. Shavrov, Dmitriy S. Kalenov, Mikhail P. Parkhomenko, Svetlana V. von Gratowski, Nooshin V. Shahmirzadi, Tavakol Pakizeh, Artemy V. Irzhak, Vladimir M. Serdyuk, Joseph A. Titovitsky, Iuliia P. Novoselova, Anton A. Komlev, Andrey E. Komlev, Dmitriy A. Kuzmin, and Igor V. Bychkov

***Abstract*—In this paper, VO_2 film on quartz substrate was prepared and investigated in an extremely high frequency (EHF) band 27–37 GHz. The study of EHF response of the nanosized VO_2 films reveals strong anomalies in the temperature range of metal-insulator transition (MIT). The intrinsic radiation of VO_2 film in the 28–32 GHz band in the vicinity of MIT was observed. Optical Raman spectra of VO_2 film perforated by micron size holes arrays were studied. The micron holes and arrays show strong change of the Raman spectra at wavelength 532 nm due to the heating by laser beam. Optical properties of homogeneous VO_2 nanospheres (NSs) were studied theoretically as well. The size effect on the optical properties of VO_2 NSs was investigated. Transition into the metallic phase caused by heating of VO_2-NSs leads to formation of localized surface plasmon resonance, which red-shifts slightly while its size increases. Increasing of NS's diameter in an insulator state leads to the appearance of a peak in the visible wavelength. The optical spectra of VO_2-NS are much broader than that of Ag-NS. This is associated with the fact that a localized electric field in the form of a dipolar mode is more intensive for Ag than in the case of VO_2.**

***Index Terms*—Antennas, Raman scattering, plasmons, nanoparticles, films, frequency dependence, electromagnetic radiation.**

Manuscript received March 15, 2018; revised July 25, 2018 and October 27, 2018; accepted January 9, 2019. Date of publication January 14, 2019; date of current version February 20, 2019. This work was supported in part by the Russian Foundation for Basic Research under Grant 17-57-560002, in part by the Iran National Science Foundation under Grant 96003683, and in part by the Act 211 Government of the Russian Federation under Contract N 02.A03.21.0011. The work of A. A. Komlev and A. E. Komlev was supported by the Russian Science Foundation under Grant 15-19-00076. This paper was presented in part at the 2nd IEEE Conference on Advances in Magnetics, Thuille, Italy, February 2018. *(Corresponding author: Alexander P. Kamantsev.)*

A. P. Kamantsev, V. V. Koledov, V. G. Shavrov, D. S. Kalenov, M. P. Parkhomenko, S. V. von Gratowski are with the Kotelnikov Institute of Radio-engineering and Electronics of RAS, Moscow 125009 Russia (e-mail: kaman4@gmail.com; victor_koledov@mail.ru; shavrov@cplire.ru; d-regus@mail.ru; m.parkhomenko@ms.ire.rssi.ru; svetlana.gratowski@yandex.ru).

N. V. Shahmirzadi and T. Pakizeh are with the Faculty of Electrical Engineering, K. N. Toosi University of Technology, Tehran 19697, Iran (e-mail: valizade@iust.elec.ac.ir; t.pakizeh@kntu.ac.ir).

A. V. Irzhak is with the National University of Science and Technology MISiS, Moscow 119049, Russia, and also with the Institute of Microelectronic Technology and High Purity Materials of RAS, Chernogolovka 142432, Russia (e-mail: airzhak@gmail.com).

V. M. Serdyuk and J. A. Titovitsky are with the Institute of Applied Physical Problems, Belarusian State University, Minsk 220045, Belarus (e-mail: serdyukvm@bsu.by; titovitsky@bsu.by).

I. P. Novoselova was with the Institute of Natural Sciences, Ural Federal University, Ekaterinburg 620002, Russia. She is now with the Faculty of Physics, University of Duisburg-Essen, Duisburg 47057, Germany (e-mail: iuliia.novoselova@uni-due.de).

A. A. Komlev and A. E. Komlev are with the Saint-Petersburg Electrotechnical University "LETI," St. Petersburg 197376, Russia, and also with the Lappeenranta University of Technology, Lappeenranta 53850, Finland (e-mail: komlevanton@hotmail.com; a.e.komlev@gmail.com).

D. A. Kuzmin and I. V. Bychkov are with the Chelyabinsk State University, Chelyabinsk 454001, Russia, and also with the South Ural State University (National Research University), Chelyabinsk 454080, Russia (e-mail: kuzminda89@gmail.com; bychkov@csu.ru).

Digital Object Identifier 10.1109/JERM.2019.2893070

I. Introduction

INVESTIGATION of the effects occurring in so-called nanoantennas (NAs) interacting with electromagnetic waves (EMW) is the matter of great interest due to the perspectives of the subsequent development of novel tunable sensors. Usually, NAs and nanoparticles (NPs) have fixed functionality; therefore, the tunability of these structures is desired in order to extend the scope of use. One of the conventional methods to obtain tunability is to exploit materials with phase transitions (PTs). Vanadium dioxide (VO_2) is known as a material having PT at near-room temperatures and its complex dielectric constant can be varied by temperature due to structural transformation accompanying metal-insulator transition (MIT). This material is an insulator at room temperature and becomes a metal above critical temperature ($T_C = 340$ K). Hence, the use of this material suggests a possibility of new applications in various fields.

In the last decade, a real breakthrough has been made in the field of nanophotonics, nanoplasmonics, NAs, and metasurfaces (optical nanomaterials). One of the main problems that the wide application of these devices faces is fixed properties during their production. Controllable devices, called "active" (not to be confused with energy generation), would not only be much more in demand but also could create new scientific and technical applications. For example, significant efforts are being made in the direction of the configurable antennas and metasurfaces [1] based on a change in carrier density of the substrate [2]–[5], "active" devices based on liquid crystals, where their effective index is varied by an electric and magnetic field [6], [7], and also electrically controlled "active" devices [8]–[10]. According to several reports, materials with MIT are the most promising materials for creating the devices with controllable properties. A detailed review of the works in this area is given in [11].

Some of the most interesting materials with MIT are oxides of certain d-elements, such as NiO, CoO, and VO_2. These materials have atomic d-shells partially filled with electrons and they are metals from the band theory point of view. However, they have a band gap in the electronic spectrum, namely Mott-Hubbard gap, with the width change under certain conditions. The MIT in VO_2 can be induced, for instance, by temperature, electric field (current and voltage), EMW or mechanical stress [12]–[20].

Possibility of observing the MIT in VO_2 on the nanoscale gives another advantage to this material, since all the applications in this paper are related to controlled NAs, nanophotonics, etc. In this regard, it should be noted that a number of papers have been published recently, where it was shown that MIT is also observed at nanosized VO_2 samples [24]–[29]. Besides, by changing the dimensions from a bulk sample to nanowires, the temperature of MIT can be reduced from 340 K to 302 K [25].

Substantial change in resistance during MIT in VO_2, or, equivalently, in the complex dielectric constant and impedance, evidently, should significantly affect the reflectance and other electro-magnetic properties over the entire wavelength range. Thus, at temperatures of MIT higher than T_c, VO_2 has a metallic conductivity with a carrier concentration of 10^{22} cm^{-3}, while its optical refractive index varies greatly from 2.5 in the monoclinic phase to 2.0 in the tetragonal phase. MIT in VO_2 is accompanied by a sudden increase in the reflection coefficient (R) of electromagnetic radiation. This rise of R is related to the change in the complex dielectric permittivity $\varepsilon = \varepsilon 1$ - i$\varepsilon 2$, which at the normal incidence of EMW is determined by the expression [30]:

$$R = |(\sqrt{\varepsilon - 1} \ - \ \sqrt{\varepsilon - 2}) \, / \, (\sqrt{\varepsilon - 1} \ + \ \sqrt{\varepsilon - 2})|^2. \quad (1)$$

The increase in the reflection coefficient occurs due to a sharp increase in the conductivity σ (T) $= \omega\varepsilon_2$ (T) / 4π and the imaginary part of the permittivity ε_2 with temperature (where ω is an angular frequency), provided that the real part of permeability is small and $\varepsilon_1 << \varepsilon_2$. A few papers have been devoted to the study of electromagnetic properties in VO_2 near MIT in the microwave range [21]–[27]. In [22] the reflection of microwave electromagnetic radiation during the MIT in VO_2 is considered. It is shown that during electromagnetic excitation by microwaves in VO_2 and its dielectric composite materials the reflection coefficient may have a jump-like increase or decrease at MIT. The value of the change depends on the field frequency and the sample thickness. The behavior of the reflection can be explained by the change of conditions for Fabry-Perot-like resonance in VO_2 film at MIT. Experimental and theoretical studies of the VO_2 microwave properties across MIT were performed [31]–[36]. Scattering parameters, including reflection, attenuation as a function of frequency and temperature, and the dependencies of these quantities on the VO_2 phase state were established [32]–[36].

Such intriguing effects of VO_2 interaction with EMW recently caused a number of works devoted to the development of controlled metamaterials and meta-surfaces based on MIT in VO_2 [37]–[46], thus, various types of metamaterial structures and their properties in different wavelength ranges were studied. In [44] some metamaterials based on localized surface plasmon resonance (LSPR) from gold and VO_2 X-band frequency range from 8 to 12 GHz were investigated. It is shown that those VO_2-based metamaterials demonstrate the tenability of electromagnetic properties in the X-band.

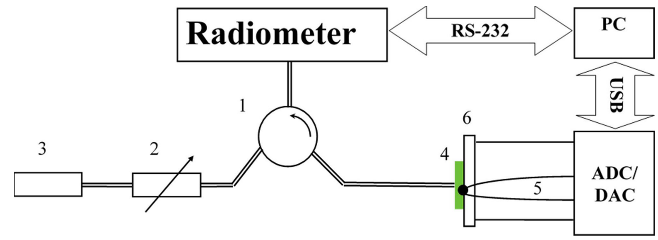

Fig. 1. Installation scheme for the PTs study using radiometer with 28–32 GHz band: 1 – the circulator; 2 – the attenuator; 3 – the cooled load (black body); 4 – the sample VO_2 thin film on the SiO_2 substrate; 5 – the thermocouple; 6 – the Peltier element with the copper surface.

The next intriguing, but less investigated topic is controllable NAs based on MIT in VO_2. In [47], a very interesting metamaterial based on gold micro- and NAs on a substrate of VO_2 for the spectral range of 0.2–2 THz was presented. In reference [48] the broadband modulation of terahertz radiation is experimentally realized by electrically controlled MIT in VO_2 in devices with a hybrid metal antenna. The devices consist of VO_2 active layers and antenna arrays. As a result, a terahertz wave with a large beam aperture ($\sim$ 0 mm) can be modulated in a wide spectral range (0.3–2.5 THz) with frequency independent modulation depth of up to 0.9. This property opens the way for realizing the multifunctional components for terahertz applications. In [49] the transmission of a THz signal through VO_2 film with NAs representing a nanopattern from an array of ordered NAs is studied. Each antenna has a length of 150 μm, and the width varies from 120 nm to 2.5 μm. The antennas are separated by a distance of 10 μm in the vertical direction and the period is 30 μm in the horizontal plane. It is shown that such a size of the elements of NAs array affects the temperature of PT in the VO_2 film.

To estimate the perspectives of using VO_2 in medical applications we formulate the following objectives of the work: synthesis of VO_2 films and investigation of their properties in the extremely high frequency (EHF) range both in reflected and intrinsic radiation modes that are of greatest interest; manufacturing of NAs - micro hole arrays as well as investigating their interaction with EMW in the visible range using Raman scattering methods; theoretical investigation of optical properties of VO_2 NSs and the temperature influence on these properties.

II. Experimental Procedure

The samples of VO_2 thin film (370 nm thickness) were obtained using a modernized setup UVN-71 equipped with a flat axial magnetron. Synthesis by reactive magnetron sputtering method was performed at direct current in argon and oxygen atmosphere. The film deposition time on a fixed SiO_2 substrate with 1.53 mm thickness is 40 minutes, the target-substrate distance is 80 mm.

The installation is designed to measure radiation of samples in 28–32 GHz band during thermal cycling in the temperature range from 273 to 393 K (see Fig. 1). The solution for measuring the intrinsic (over thermal) radiation of the sample in the vicinity of MIT in vacuum or air is described in works [50],

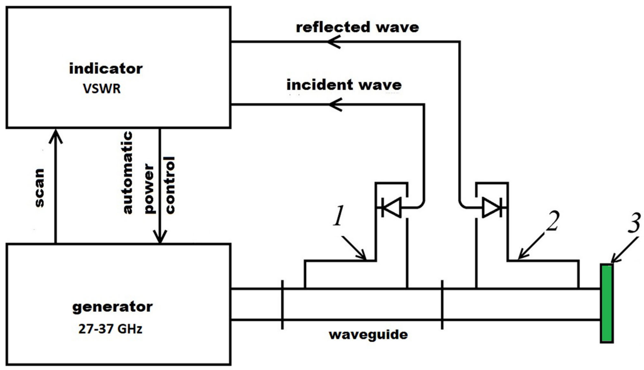

Fig. 2. Block diagram of the installation for measuring the reflection coefficient: 1 – the directional coupler and detector head of the incident wave; 2 – the directional coupler and detector head of the reflected wave; 3 – the sample of VO_2 thin film on the SiO_2 substrate.

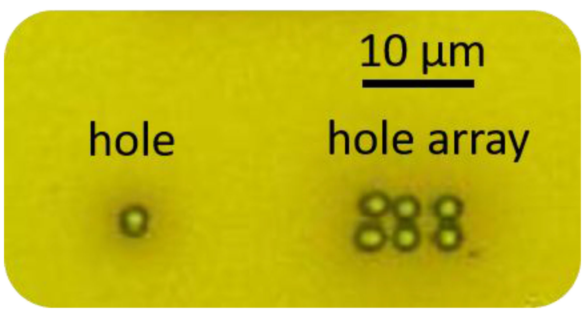

Fig. 3. The holes and hole array produced by FIB milling in the surface of VO_2 370 nm thick film prepared on SiO_2 substrate.

[51]. Sample (4) undergoes the PT as a result of heating and cooling by the Peltier element (6), the sample temperature is controlled by the thermocouple (5). Not only the sample (4), but also the radiometer is the source of thermal radiation. Thermal radiation generated by the radiometer is fed into the waveguide (7.2×3.4 mm) and through the circulator (1) falls on the cooled load (the black body) (3). The radiation of the load is cooled down by liquid nitrogen (less intense than the radiometer radiation) and through the attenuator (2) and the circulator (1) falls on the sample (4). Attenuator (2) regulates the ratio between the "cold" radiation of the load and the "warm" room radiation incident on the sample. This radiation is partially reflected from the sample and goes back into the radiometer along with its own radiation. The contributions from intrinsic and reflected radiation are separated by the difference of the measurement techniques.

To measure the reflection coefficient of the VO_2 samples near MIT, the standard panoramic sweep-frequency reflectometer R2-65 with the oscillating frequency generator 27–37 GHz, and the indicator unit Ya2R-67 of voltage standing wave ratio (VSWR) were used. The cross-section of rectangular standard waveguides was 7.2×3.4 mm. The scheme of the experiment is shown in Fig. 2.

The Raman scattering spectra were obtained on the Raman spectrometer Senterra from Brucker. To excite the Raman spectrum radiation a laser with a wavelength of 532 nm and a variable power of 2–20 mW was used. The accumulation time of the

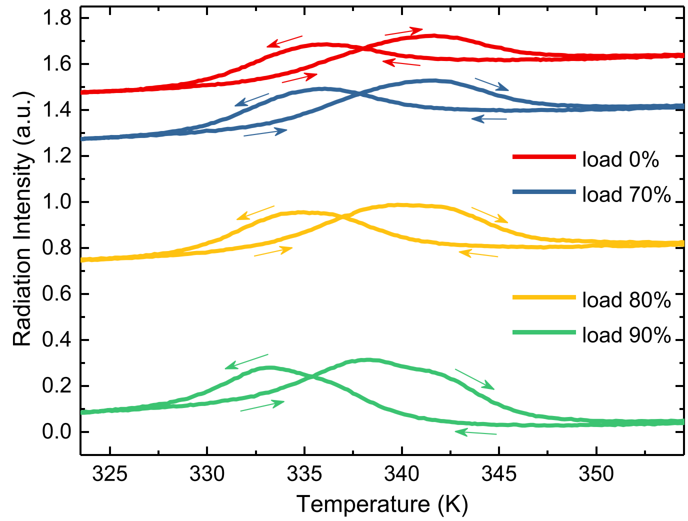

Fig. 4. Temperature dependence of radiation intensity of the thin VO_2 film obtained in 28–32 GHz band by radiometer under backlight load: from 90% down to 0% of the "cold" radiation from the load–the blackbody cooled by liquid nitrogen. The ratio of "cold" and "warm" radiation is regulated by the attenuator.

signal at the point was 15 times per 25 s. After subtraction of the background the spectra were normalized. In the case of VO_2, properties of which depend on the phase composition, it is possible to observe the effects of power of laser incident radiation on the measured spectra.

III. Results and Discussion

A. *Intrinsic Radiation in the Area of MIT on 28–32 GHz Band*

We have investigated the intrinsic radiation of VO_2 sample by the method represented in Fig. 1. The VO_2 sample was irradiated with illumination of different brightness temperature: from 90% to 0% of "cold" radiation from the load - a blackbody cooled by nitrogen. The ratio of "cold" and "warm" radiation was regulated by the attenuator. In the presence of "warm" room radiation (nitrogen load 0–70%) the signal level in the radiometer grows linearly with temperature, although in the region of MIT a sharp increase in intensity of 15% was observed, accompanied by temperature hysteresis (see Fig. 4).

The intensity of these radiation anomalies (in absolute value) in VO_2 with MIT does not change from the boiling point of liquid nitrogen to room temperature with increase of the brightness temperature of the illumination. In previously studied alloys with structural PT, such as Ni-Mn-Ga-Fe [49] and Ti-Ni-Cu [51], the intensity of radiation anomalies recorded by the radiometer, was decreasing with increasing brightness temperature of the illumination. It can be an indication of the different nature of intrinsic radiation at PT in intermetallic alloys and VO_2 films.

B. *Reflectance in Vicinity of MIT on 27–37 GHz Band*

The hysteretic behavior of EMW reflection coefficient of the VO_2 film is shown for direct and inverse MIT using setup described in Fig. 2. It was found that the thin VO_2 film on SiO2 substrate with a shielding layer of a conductor could have an in-

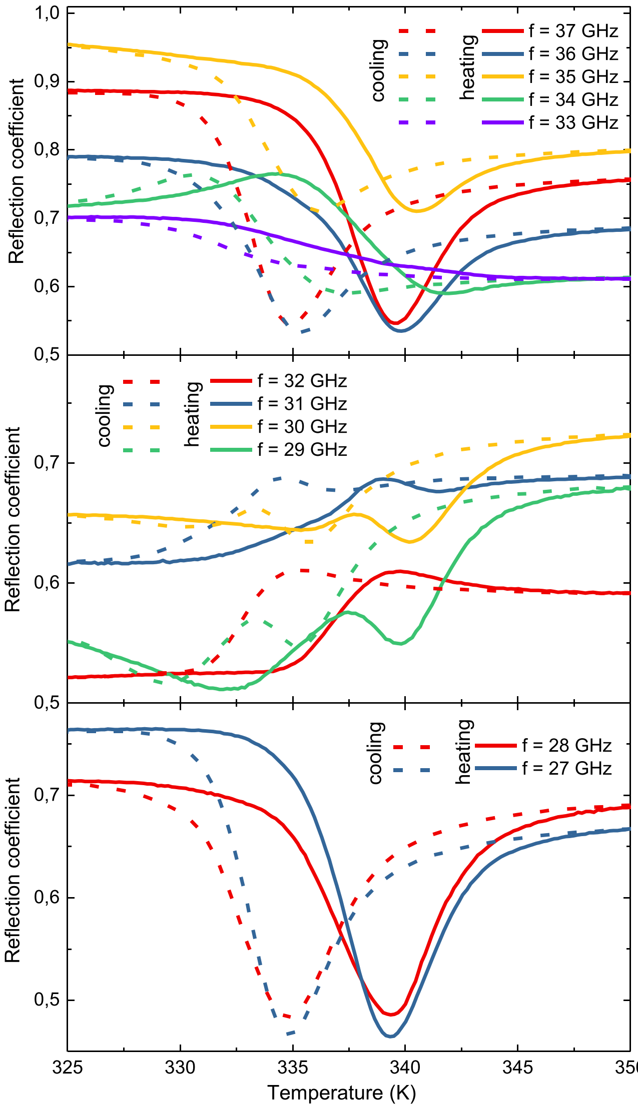

Fig. 5. Temperature dependence of the reflection coefficient recorded on a panoramic reflectometer at different frequencies from 27 to 37 GHz.

verse hysteresis of reflectance in frequency range of 29–32 GHz (for the frequencies out of this range temperature dependencies of reflectance have a dip, while in this frequency range they have a peak). This effect may be observed for the temperature near the MIT (see Fig. 5).

To explain the observed effect a theoretical model has been proposed. The investigated structure is VO_2-quartz-copper. The copper is considered to be perfectly conductive (everything is reflected), the quartz does not have frequency dispersion and the dielectric constant ($\varepsilon = 3.8$ [52]) does not change with temperature. The VO_2 behavior is modeled by Drude theory with the plasma frequency and the collision frequency of electrons depending on the temperature. For estimation we consider the temperature dependence (at heating) like piecewise continuous form [53].

The approximation is rough, but suitable for qualitative description. The results of the calculations are shown in Fig. 6. It can be seen that the qualitatively temperature dependence of the

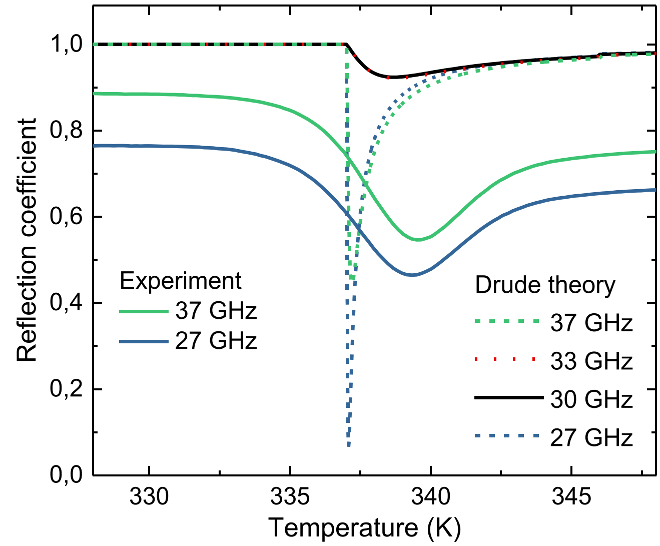

Fig. 6. Temperature dependence of the reflection coefficient at different frequencies in the range of 27–37 GHz for VO_2 film on SiO_2 substrate at heating (the modelling in the frame of the Drude theory [53] and comparison with experimental data).

reflection coefficient satisfactorily describes the measurement results. The dip on the curves is associated with the excitation of plasmon resonance in the VO_2 film: plasma frequency increases, and at a certain temperature becomes comparable with the frequency of EMW in the waveguide. This is indirectly confirmed by the fact that the temperature of the dips in Fig. 6 increases with frequency increase (plasma frequency also increases with the temperature). The width and depth of the dips depends mainly on the collision frequency of the electrons. Therefore, the dips disappearance may be due to the fact that the collision frequency in the sample becomes comparable or greater than the EMW frequency. It is necessary that these values should be at the same temperatures when plasmon resonance occurs. Further investigation is necessary in order to understand the nature of this effect.

C. Raman Spectra of NAs Based on VO_2

The spectra obtained from the structure formed by two adjacent holes in the VO_2 film (see Fig. 3) and the surface of the film show differences: the relative intensity of the 620 cm^{-1} peak obtained in the region of the bridge between the holes is much smaller than that of the analogous peak in the spectrum, obtained on the film (see Fig. 7). A shift toward smaller wave numbers was observed, the peak is at the position of 614 cm^{-1} from the bridge region and 622 cm^{-1} from the surface of the film. This behavior of the peak is possibly related to the mechanical stresses that have arisen in the region of the bridge.

Fig. 8 shows spectra obtained after irradiating the surface of the VO_2 film with different power of laser radiation (2, 10, and 20 mW). On the spectrum obtained after irradiation with a laser of 20 mW it is seen that there are additional peaks at positions 146, 284, 531, 703 and 997 cm^{-1}, compared with the unirradiated one. These peaks may appear due to the photoinduced production of the VO_2 metallic phase [54].

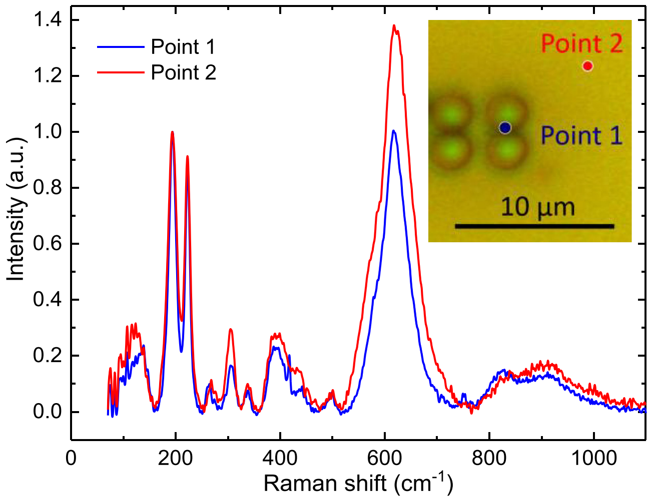

Fig. 7. Raman spectrum shift from the VO_2 sample defined in the inset from the bridge between the holes (Point 1) and from the film surface (Point 2). The laser power is 2 mW.

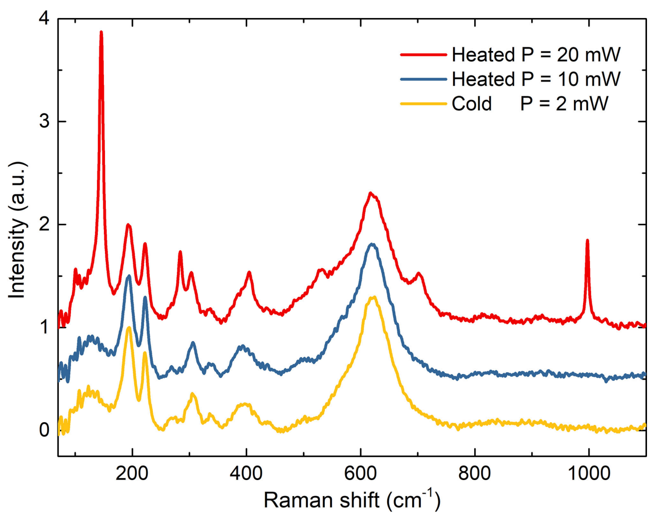

Fig. 8. Raman spectrum shift of VO_2 film before heating (cold), after laser irradiating with 10 mW laser power (heated 10 mW), and after laser irradiating with 20 mW laser power (heated 20 mW).

D. Properties of VO_2 NS in Optical Spectrum

Optical properties of VO_2 NSs are studied theoretically by exploiting various methods such as dipole approximation (DA), modified long wavelength approximation (MLWA) and Mie theory. In order to investigate the temperature effect on these characteristics, the temperature dependent dielectric constant of VO_2 is adopted from experimental data in [55] and is also shown in Fig. 9. The NS in simulations is surrounded by air.

E. Dipole Approximation

Optical responses of VO_2 NSs with optical constant $\varepsilon = \varepsilon_1 + i\varepsilon_2$, immersed in a medium with permittivity of ε_m, are simply computed by the dipole approximation (DA). Notice that the NS size must be much smaller than the wavelength (<1% wavelength). The real (ε_1) and imaginary parts (ε_2) of VO_2 dielectric constants above and below T_c are shown in Fig. 9. By

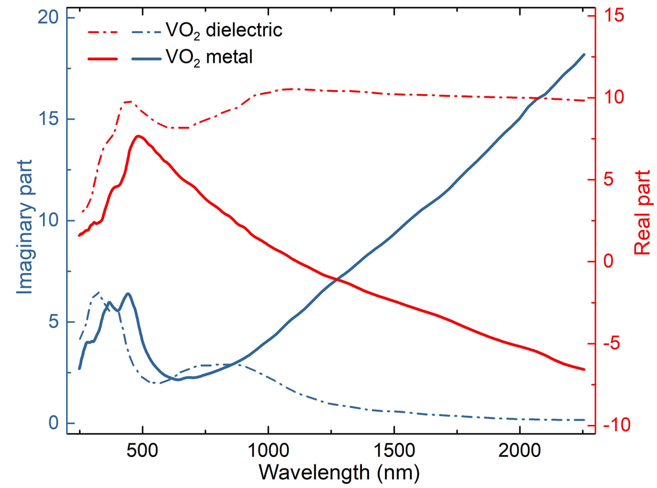

Fig. 9. Experimental dielectric constant of VO_2 below and above the T_c, extracted from [55].

applying this method the absorption, scattering and extinction cross sections are expressed respectively as follows:

$$C_{\rm abs} = k{\rm Im}\{\alpha\}, C_{\rm sca} = \frac{k^4}{6\pi}|\alpha|^2, C_{\rm ext} = C_{\rm abs} + C_{\rm sca} \quad (2)$$

where k is the wave number and α is polarizability coefficient of NS obtained in [56] by

$$\alpha = 4\pi a^3 \frac{\varepsilon - \varepsilon_m}{\varepsilon + 2\varepsilon_m}. \quad (3)$$

The parameter a is the NS radius. The dimensionless optical efficiencies are computed as follows:

$$Q_i = \frac{C_i}{A} \quad i \in \{{\rm abs}, {\rm sca}, {\rm ext}\} \quad (4)$$

where A is a geometrical cross-section illuminated by the incident light. This parameter corresponds to πa^2. The polarizability experiences a resonant enhancement when the $(|\varepsilon + 2\varepsilon_{\rm m}|)$ is minimized, which for small or slowly varying ε_2 simplifies to $\varepsilon = -2\varepsilon_{\rm m}$ (Fröhlich condition) [57]. This enhancement is observed in metallic phase of VO_2 NS at 355 K. In this case, the real part of dielectric constant becomes negative, as it can be seen in Fig. 9.

F. Modified Long Wavelength Approximation

As the NSs radius increases, the DA loses its accuracy and it is not applicable. However, by using the modified polarizability ($\tilde{\alpha}$) DA can be utilized for NSs in which dimensions are less than 10% of wavelength. By calculating the modified $\tilde{\alpha}$, the optical cross sections and efficiencies can be obtained by Eq. 2. The modified polarizability is expressed in [58] as

$$\tilde{\alpha} = \frac{\alpha}{1 - \frac{2}{3}ik^3\alpha - \frac{1}{a}k^2\alpha}. \quad (5)$$

G. The Mie Theory

The Mie theory is a powerful method for computing the optical properties of NSs. In this procedure, the electromagnetic

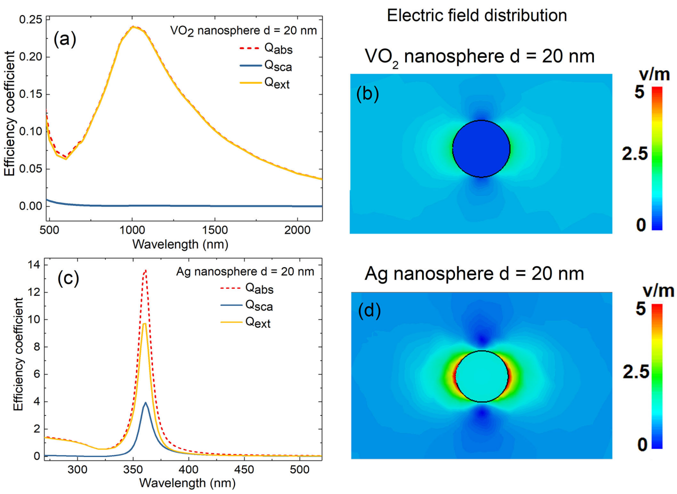

Fig. 10. Optical efficiency coefficients (a) and electric-field distribution (b) of a VO_2 NS-20 nm at $T = 355$ K. Optical efficiency (c) and the electric-field distribution (d) of an Ag NS-20 nm.

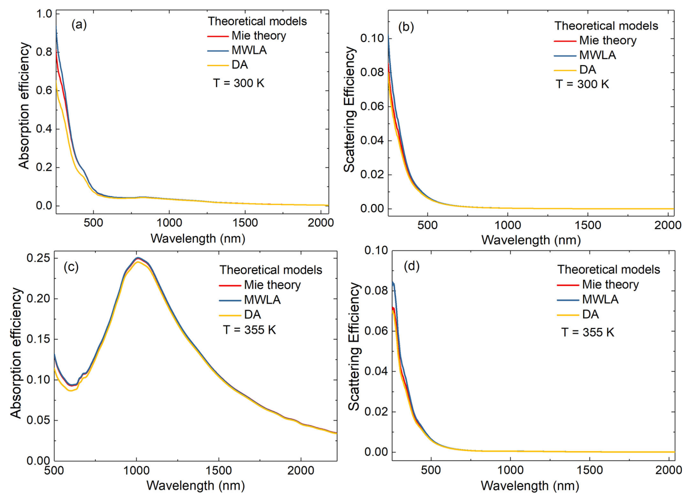

Fig. 11. Optical properties of a VO_2 NS-20 nm (a) and (b) below T_c, and (c) and (d) above T_c.

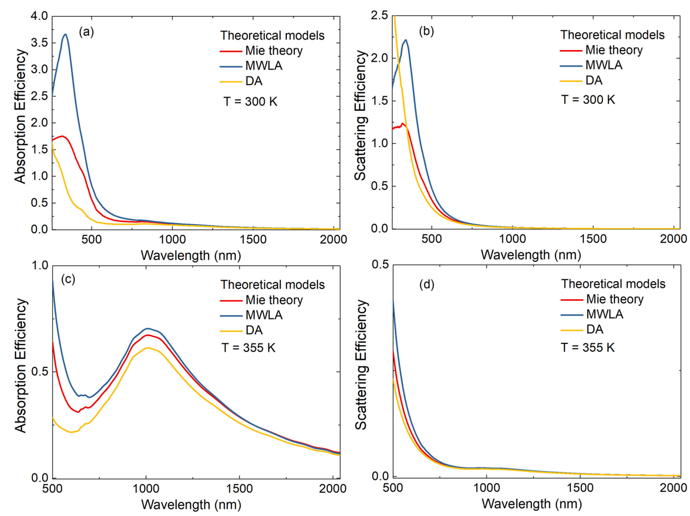

Fig. 12. Optical properties of a VO_2 NS-50 nm (a) and (b) below T_c, and (c) and (d) above T_c.

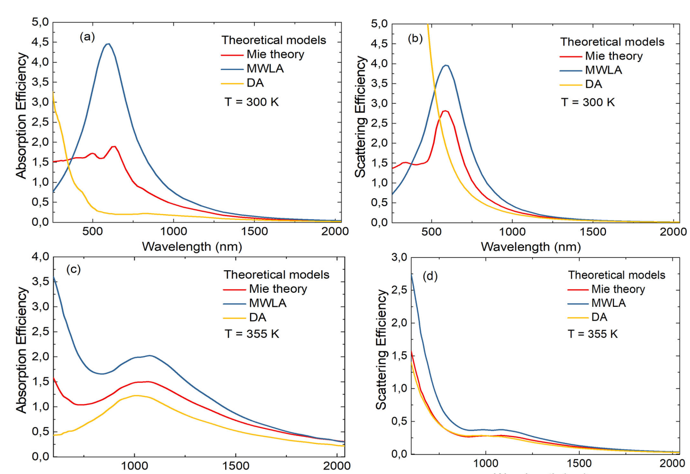

Fig. 13. Optical properties of a VO_2 NS-100 nm (a) and (b) below T_c, and (c) and (d) above T_c.

fields are described by spherical harmonics in spherical coordinates. By satisfying the boundary conditions and calculating the scattering coefficients $\{a_n, b_n\}$ the optical cross sections are achieved as follows:

$$C_{\text{ext}} = \frac{2\pi}{k^2} \sum_{n=1}^{\infty} (2n+1) \operatorname{Re}\left[a_n + b_n\right]$$

$$C_{\text{sca}} = \frac{2\pi}{k^2} \sum_{n=1}^{\infty} (2n+1) \left(|a_n|^2 + |b_n|^2 \right) \tag{6}$$

where n is the order of Riccati-Bessel functions [56]. In order to obtain optical efficiencies, (4) is used [56].

The optical efficiencies and electric field distribution of a 20 nm nanosphere in metallic phase are presented in Fig. 10(a,b) and are compared with the same Ag nanosphere of the same dimension [see Fig. 10(c) and (d)]. At the wavelength of 1 μm a resonance peak is observed in spectra of VO_2 in metallic phase. Due to the electric field distribution, the origin of this resonance is an electric dipole. The enhancement of Ag in LSPR is much higher than VO_2 in metallic phase. However, there is a little change in LSPR of Ag NS when the particles are heated from room temperature up to 773 K [59]. It is obvious that the principle of resonance around 1000 nm is LSPR. By decreasing the temperature LSPR disappears. Therefore, this resonance can be switched thermally as can be seen in Fig. 11(a) and (b).

In order to investigate the size effects on optical properties of VO_2 NSs in insulator and metallic phase optical absorption and scattering efficiencies of 20 nm, 50 nm and 100 nm are calculated. The results are presented in Figs. 11–13. In the metallic phase $(T = 355\,\text{K})$ the optical efficiencies are remarkable at the wavelength of 1000 nm for NS-20 nm [see Fig. 11(c)]. By decreasing the temperature VO_2 experiences MIT, and eventually becomes insulator. The LSPR peak which is observed in metallic phase vanishes, and also a peak in the optical spectra for both NS-50 nm and NS-100 nm appears in the visible range.

This peak can be associated with the combined modes. In the metallic phase LSPR redshifts and broadens slightly as the radius of NS increases, which occurs at 1011 nm and 1064 nm for 50 nm and 100 nm NSs, respectively. This phenomenon can be simply understood from dipole approximation. LSPR is obvious in scattering spectra for $r \geq 100$ nm. As usually, the absorption efficiency is higher than the scattering near the LSPR peaks in all cases.

IV. Conclusions

This complex investigation significantly clarifies the understanding of VO_2 behavior under optical and EHF waves. The obtained results allow, particularly, estimate the perspectives of using VO_2 in medical applications. For instance, effective therapy for malignant neoplasms is a major unresolved challenge in modern medicine. It may be addressed by using metallic NPs, introduced at the affected site to be irradiated with the near-infrared light. Radiation causes heating of NPs and transfer of the heat to cancer cells destroying them. The VO_2 NPs seem to be more perspective for applications than pure metallic NPs due to the possibility to control its properties using MIT.

The optical properties of noble metallic nanoparticles such as Ag are independent from the temperature. There is a little change in LSPR of Ag-NS when the particles are heated from room temperature up to 773 K. Thus, their properties and the LSPR wavelength are fixed after they are created. Individual VO_2 NS experiences LSPR at wavelength about 1 μm which can be switched thermally. The combination of noble metallic nanoparticles with VO_2 as core-shell structures or locating the noble metallic nanoparticles in VO_2 environment gives tunability upon optical properties and also LSPR wavelength. For example, the optical absorption spectra of Au nanoparticles are narrower and more remarkable outside of the near-infrared region. The laser light of wavelengths above or below the near-infrared range is significantly absorbed by water or hemoglobin, respectively. The aforementioned structures show a red shift and thus could expand the absorption spectrum of noble metallic nanoparticles, which is desired in such a treatment like cancer cells ablation.

References

[1] N. I. Zheludev and E. Plum, "Reconfigurable nanomechanical photonic metamaterials," *Nature Nanotechnol.*, vol. 11, no. 1, pp. 16–22, 2016.

[2] H.-T. Chen *et al.*, "Experimental demonstration of frequency-agile terahertz metamaterials," *Nature Photon.*, vol. 2, no. 5, pp. 295–298, 2008.

[3] Y. C. Jun, E. Gonzales, J. L. Reno, E. A. Shaner, A. Gabbay, and I. Brener, "Active tuning of mid-infrared metamaterials by electrical control of carrier densities," *Opt. Exp.*, vol. 20, no. 2, pp. 1903–1911, 2012.

[4] H.-T. Chen, W. J. Padilla, M. J. Cich, A. K. Azad, R. D. Averitt, and A. J. Taylor, "A metamaterial solid-state terahertz phase modulator," *Nature Photon.*, vol. 3, no. 3, pp. 148–151, 2009.

[5] H. T. Chen, W. J. Padilla, J. M. O. Zide, A. C. Gossard, A. J. Taylor, and R. D. Averitt, "Active terahertz metamaterial devices," *Nature*, vol. 444, no. 7119, pp. 597–600, 2006.

[6] Q. Zhao *et al.*, "Electrically tunable negative permeability metamaterials based on nematic liquid crystals," *Appl. Phys. Lett.*, vol. 90, no. 1, 2007, Art. no. 011112.

[7] F. L. Zhang *et al.*, "Electrically controllable fishnet metamaterial based on nematic liquid crystal," *Opt. Exp.*, vol. 19, no. 2, pp. 1563–1568, 2011.

[8] V. Stockhausen *et al.*, "Giant plasmon resonance shift using poly (3, 4-ethylenedioxythiophene) electrochemical switching," *J. Amer. Chem. Soc.*, vol. 132, no. 30, pp. 10224–10226, 2010.

[9] J. Berthelot *et al.*, "Tuning of an optical dimer nanoantenna by electrically controlling its load impedance," *Nano Lett.*, vol. 9, no. 11, pp. 3914–3921, 2009.

[10] W. Dickson, G. A. Wurtz, P. R. Evans, R. J. Pollard, and A. V. Zayats, "Electronically controlled surface plasmon dispersion and optical transmission through metallic hole arrays using liquid crystal," *Nano Lett.*, vol. 8, no. 1, pp. 281–286, 2008.

[11] Z. Yang, C. Ko, and S. Ramanathan, "Oxide electronics utilizing ultrafast metal-insulator transitions," *Annu. Rev. Mater. Res.*, vol. 14, pp. 337–367, 2011.

[12] S. Lysenko, V. Vikhnin, A. Rúa, F. Fernández, and H. Liu, "Critical behavior and size effects in light-induced transition of nanostructured VO_2 films," *Phys. Rev. B*, vol. 82, no. 20, 2010, Art. no. 205425.

[13] C. Chen, R. Wang, L. Shang, and C. Guo, "Gate-field-induced phase transitions in VO_2: Monoclinic metal phase separation and switchable infrared reflections," *Appl. Phys. Lett.*, vol. 93, no. 17, 2008, Art. no. 171101.

[14] M. Rini *et al.*, "Photoinduced phase transition in VO_2 nanocrystals: Ultrafast control of surface-plasmon resonance," *Opt. Lett.*, vol. 30, no. 5, pp. 558–560, 2005.

[15] S. Lysenko, A. J. Rua, V. Vikhnin, J. Jimenez, F. Fernandez, and H. Liu, "Light-induced ultrafast phase transitions in VO_2 thin film," *Appl. Surf. Sci.*, vol. 252, no. 15, pp. 5512–5515, 2006.

[16] H. Guo *et al.*, "Mechanics and dynamics of the strain-induced M1-M2 structural phase transition in individual VO_2 nanowires," *Nano Lett.*, vol. 11, no. 8, pp. 3207–3213, 2011.

[17] A. Cavalleri *et al.*, "Femtosecond structural dynamics in VO_2 during an ultrafast solid-solid phase transition," *Phys. Rev. Lett.*, vol. 87, no. 23, 2001, Art. no. 237401.

[18] A. B. Ilyinskiy, O. E. Kvashenkina, and E. B. Shadrin, "Phase transition and correlation effects in vanadium dioxide," *Semiconductors*, vol. 46, no. 4, pp. 422–429, 2012.

[19] G. Stefanovich, A. Pergament, and D. Stefanovich, "Electrical switching and Mott transition in VO_2," *J. Phys., Condens. Matter*, vol. 12, no. 41, pp. 8837–8845, 2000.

[20] Y. Zhou, X. Chen, C. Ko, Z. Yang, C. Mouli, and S. Ramanathan, "Voltage-triggered ultrafast phase transition in vanadium dioxide switches," *IEEE Electron Device Lett.*, vol. 34, no. 2, pp. 220–222, Feb. 2013.

[21] C. Kübler *et al.*, "Coherent structural dynamics and electronic correlations during an ultrafast insulator-to-metal phase transition in VO_2," *Phys. Rev. Lett.*, vol. 99, no. 11, 2007, Art. no. 116401.

[22] J. Yoon *et al.*, "Controlling the temperature and speed of the phase transition of VO_2 microcrystals," *ACS Appl. Mater. Interfaces*, vol. 8, no. 3, pp. 2280–2286, 2016.

[23] R. Lopez, T. E. Haynes, L. A. Boatner, L. C. Feldman, and R. F. Haglund, "Size effects in the structural phase transition of VO_2 nanoparticles," *Phys. Rev. B*, vol. 65, no. 22, 2002, Art. no. 224113.

[24] H. Liu *et al.*, "Size effects on metal-insulator phase transition in individual vanadium dioxide nanowires," *Opt. Exp.*, vol. 22, no. 25, pp. 30748–30755, 2014.

[25] E. U. Donev, J. I. Ziegler, R. F. Haglund, and L. C. Feldman, "Size effects in the structural phase transition of VO_2 nanoparticles studied by surface-enhanced Raman scattering," *J. Opt. A, Pure Appl. Opt.*, vol. 11, no. 12, 2009, Art. no. 125002.

[26] K. Appavoo and R. F. Haglund Jr., "Detecting nanoscale size dependence in VO_2 phase transition using a split-ring resonator metamaterial," *Nano Lett.*, vol. 11, no. 3, pp. 1025–1031, 2011.

[27] V. R. Morrison *et al.*, "A photoinduced metal-like phase of monoclinic VO_2 revealed by ultrafast electron diffraction," *Science*, vol. 346, no. 6208, pp. 445–448, 2014.

[28] D. Wegkamp *et al.*, "Instantaneous band gap collapse in photoexcited monoclinic VO_2 due to photocarrier doping," *Phys. Rev. Lett.*, vol. 113, no. 21, 2014, Art. no. 216401.

[29] M. Liu *et al.*, "Terahertz-field-induced insulator-to-metal transition in vanadium dioxide metamaterial," *Nature*, vol. 487, no. 7407, pp. 345–348, 2012.

[30] Y. K. Kovneristy, I. Y. Lazareva, and A. A. Ravaev, *Materials Absorbing Microwave Radiation*, Moscow, Russia: Nauka (in Russian), 1982.

[31] B. M. Gorelov, K. P. Konin, V. V. Koval, and V. M. Ogenko, "A change in the microwave radiation reflection upon a dielectric–metal transition in vanadium dioxide," *Tech. Phys. Lett.*, vol. 27, no. 2, pp. 157–159, 2001.

[32] S. Beeson, J. Dickens, and A. Neuber, "A high power microwave triggered RF opening switch," *Rev. Sci. Instrum.*, vol. 86, no. 3, 2015, Art. no. 034704.

[33] F. Dumas-Bouchiat, C. Champeaux, and A. Catherinot, "RF-microwave switches based on reversible semiconductor-metal transition of VO_2 thin films synthesized by pulsed-laser deposition," *Appl. Phys. Lett.*, vol. 91, no. 22, 2007, Art. no. 223505.

[34] J. Givernaud *et al.*, "Microwave power limiting devices based on the semiconductor–metal transition in vanadium–dioxide thin films," *IEEE Trans. Microw., Theory Techn.*, vol. 58, no. 9, pp. 2352–2361, Sep. 2010.

[35] K. C. Pan, W. Wang, E. Shin, K. Freeman, and G. Subramanyam, "Vanadium oxide thin-film variable resistor-based RF switches," *IEEE Trans. Electron Devices*, vol. 62, no. 9, pp. 2959–2965, Sep. 2015.

[36] T. S. Jordan *et al.*, "Model and characterization of VO_2 thin-film switching devices," *IEEE Trans. Electron Devices*, vol. 61, no. 3, pp. 813–819, Mar. 2014.

[37] M. J. Dicken *et al.*, "Frequency tunable near-infrared metamaterials based on VO_2 phase transition," *Opt. Exp.*, vol. 17, no. 20, pp. 18330–18339, 2009.

[38] T. Driscoll *et al.*, "Dynamic tuning of an infrared hybrid-metamaterial resonance using vanadium dioxide," *Appl. Phys. Lett.*, vol. 93, no. 2, 2008, Art. no. 024101.

[39] A. Crunteanu, G. Humbert, J. Leroy, L. Huitema, J.-C. Orlianges, and A. Bessaudou, "Tunable THz metamaterials based on phase-changed materials (VO_2) triggered by thermal and electrical stimuli," *Terahertz, RF, Millimeter, Submillimeter-Wave Technol. Appl. X.–Int. Soc. Opt. Photon.*, vol. 10103, 2017, Art. no. 101031H.

[40] H. Liu, J. Lu, and X. R. Wang, "Metamaterials based on the phase transition of VO_2," *Nanotechnol.*, vol. 29, no. 2, 2017, Art. no. 024002.

[41] J. Leroy, G. Humbert, J.-C. Orlianges, C. Champeaux, P. Blondy, and A. Crunteanu, "Tunable terahertz metamaterials based on hybrid integration of the VO_2 metal-insulator transition material," in *Proc. 8th Int. Conf. Adv. Mater.*, 2015.

[42] H. Kim, N. Charipar, E. Breckenfeld, A. Rosenberg, and A. Piquéa, "Active terahertz metamaterials based on the phase transition of VO_2 thin films," *Thin Solid Films*, vol. 596, pp. 45–50, 2015.

[43] J. H. Shin, K. H. Park, and H. C. Ryu, "Electrically controllable terahertz square-loop metamaterial based on VO_2 thin film," *Nanotechnol.*, vol. 27, no. 19, 2016, Art. no. 195202.

[44] G. Zhang, H. Ma, C. Lan, R. Gao, and J. Zhou, "Microwave tunable metamaterial based on semiconductor-to-metal phase transition," *Sci. Rep.*, vol. 7, no. 1, 2017, Art. no. 5773.

[45] X. Zheng, Z. Xiao, and X. Ling, "A tunable hybrid metamaterial reflective polarization converter based on vanadium oxide film," *Plasmonics*, vol. 13, no. 1, pp. 287–291, 2018.

[46] X. Wen, Q. Zhang, J. Chai, L. M. Wong, S. Wang, and Q. Xiong, "Near-infrared active metamaterials and their applications in tunable surface-enhanced Raman scattering," *Opt. Exp.*, vol. 22, no. 3, pp. 2989–2995, 2014.

[47] Z. J. Thompson *et al.*, "Terahertz-triggered phase transition and hysteresis narrowing in a nanoantenna patterned vanadium dioxide film," *Nano Lett.*, vol. 15, no. 9, pp. 5893–5898, 2015.

[48] C. Han, E. P. J. Parrott, G. Humbert, A. Crunteanu, and E. Pickwell-MacPherson, "Broadband modulation of terahertz waves through electrically driven hybrid bowtie antenna-VO_2 devices," *Sci. Rep.*, vol. 7, no. 1, 2017, Art. no. 12725.

[49] Y.-G. Jeong *et al.*, "Terahertz nano antenna enabled early transition in VO_2," arXiv:1208.3269, 2012.

[50] I. Bychkov *et al.*, "Electromagnetic waves generation in $Ni_{2.14}Mn_{0.81}GaFe_{0.05}$ Heusler alloy at structural phase transition," *Acta Physica Polonica A*, vol. 127, no. 2, pp. 588–590, 2015.

[51] I. V. Bychkov *et al.*, "The intrinsic radiation and electromagnetic wave reflection coefficient in the range of 8 mm of $Ni_{2.14}Mn_{0.81}GaFe_{0.05}$ and Ti-Ni alloys in the temperature interval near the phase transitions of the 1st and 2nd order," *J. Radio electron.* no. 12, p. 13, 2014.

[52] P. Sarafis and A. G. Nassiopoulou, "Dielectric properties of porous silicon for use as a substrate for the on-chip integration of millimeter-wave devices in the frequency range 140 to 210 GHz," *Nanoscale Res. Lett.*, vol. 9, no. 1, p. 13, 2014.

[53] T. Peterseim, M. Dressel, M. Dietrich, and A. Polity, "Optical properties of VO_2 films at the phase transition: Influence of substrate and electronic correlations," *J. Appl. Phys.*, vol. 120, no. 7, 2016, Art. no. 075102.

[54] V. S. Vikhnin, I. N. Goncharuk, V. Yu. Davydov, F. A. Chudnovskii, and E. B. Shadrin, "Raman spectra of the high-temperature phase of vanadium dioxide and model of structural transformations near the metal-semiconductor phase transition," *Phys. Solid State*, vol. 37, no. 12, pp. 1971–1978, 1995.

[55] H. W. Verleur, A. S. Barker, Jr., and C. N. Berglund, "Optical properties of VO_2 between 0.25 and 5 eV," *Phys. Rev.*, vol. 172, no. 3, pp. 788–798, 1968.

[56] C. F. Bohren and D. R. Huffman, *Absorption and Scattering of Light by Small Particles*. Hoboken, NJ, USA: Wiley, 2008.

[57] S. A. Maier, *Plasmonics: Fundamentals and Applications*. New York, NY, USA: Springer, 2007.

[58] K. L. Kelly, E. Coronado, and L. L. Zhao, "The optical properties of metal nanoparticles: The influence of size, shape, and dielectric environment," *J. Phys. Chem. B.*, vol. 107, no. 3, pp. 668–677, 2003.

[59] R. H. Doremus, "Optical properties of small silver particles," *J. Chem. Phys.*, vol. 42, no. 1, pp. 414–417, 1965.

Authors' photographs and biographies not available at the time of publication.